Electronic Supplementary Information for

Synaptic Plasticity and Learning Behaviors in Flexible Artificial Synapse Based on Polymer/Viologen System

Chaochao Zhang,[abc†] Yu-Tsung Tai,[d†] Jie Shang,[ab†] Gang Liu,[*ab] Kun-Li Wang,[*d] Chienwen Hsu,[d] Xiaohui Yi,[ab] Xi Yang,[ab] Wuhong Xue,[ab] Hongwei Tan,[ab] Shanshan Guo,[ab] Liang Pan[ab] and Run-Wei Li[*ab]

[a]*Key Laboratory of Magnetic Materials and Devices, Ningbo Institute of Materials Technology and Engineering, Chinese Academy of Sciences, Ningbo 315201, P. R. China.*
[b]*Zhejiang Province Key Laboratory of Magnetic Materials and Application Technology, Ningbo Institute of Materials Technology and Engineering, Chinese Academy of Sciences, Ningbo 315201, P. R. China.*
[c]*Department of Chemistry, Shanghai University, Shanghai 200444, P. R. China.*
[d]*Department of Chemical Engineering and Biotechnology, National Taipei University of Technology, Taipei 10608, Taiwan.*
E-mail: liug@nimte.ac.cn (Prof. Dr. G. Liu), runweili@nimte.ac.cn (Prof. Dr. R.-W. Li), klwang@ntut.edu.tw (Prof. Dr. K.-L. Wang)

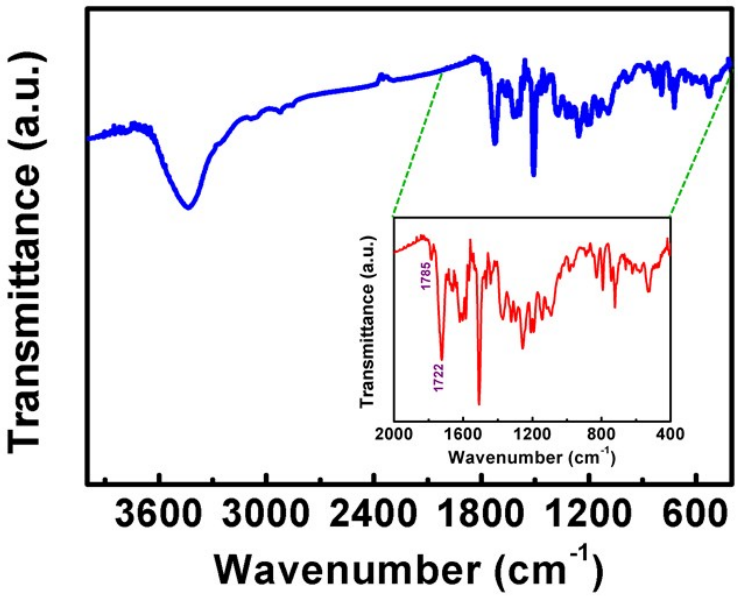

Figure S1. Fourier transformed infrared (FT-IR) spectrum of TPA-PI. The broad peak of 3450 cm^{-1} is attributed to the moisture.

The polycondensation was carried out at ambient temperature to form the corresponding poly(amic acid)s, and followed by chemical cyclodehydration. The polymer structure was confirmed by FT-IR and NMR spectrum. The polyimide showed the characteristic absorption bands of the imide ring at around 1785 cm^{-1} (asymmetric C=O stretch) and 1722 cm^{-1} (symmetric C=O stretch), while the characteristic absorptions at 3384 and 3472 cm^{-1} for the amino groups of the diamine monomer (ATATPy) disappeared.

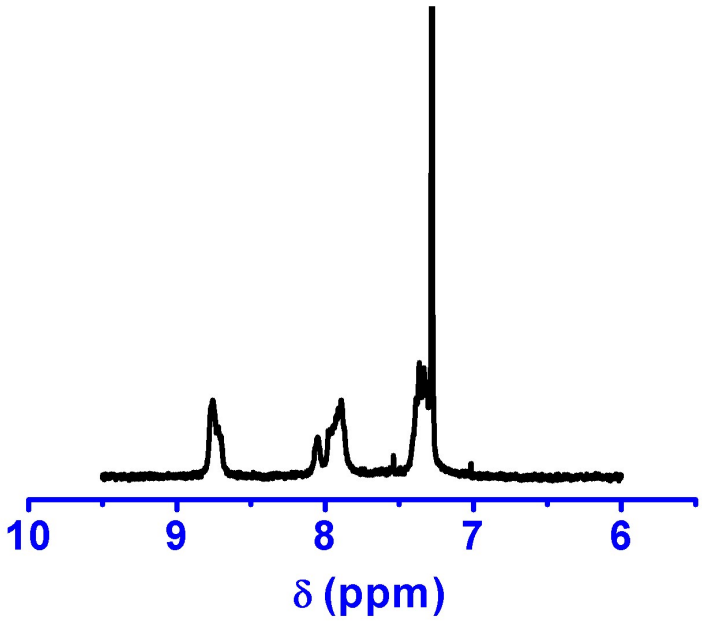

Figure S2. ^{1}H NMR spectrum of TPA-PI. The strongest single peak (δ7.28) is the residual solvent peak of $CDCl_3$.

The ^{1}H NMR spectrum of the polymer is shown in Fig. S2. The amino peak for the ATATPy diamine at 5.08 ppm in ^{1}H NMR spectrum disappeared and the integration ratio of the aromatic protons satisfied the polyimide structure. The FT-IR and NMR spectra of the polyimide suggest that polymerization has been carried out efficiently and successfully.

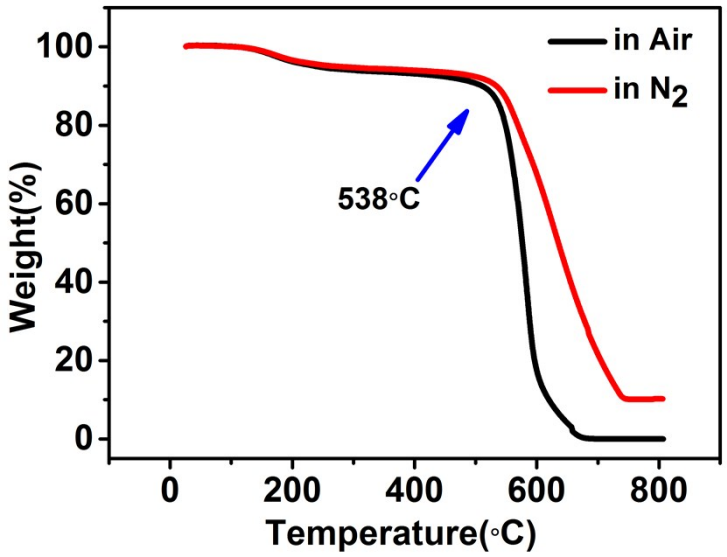

Figure S3. Thermogravimetric analysis (TGA) curves of triphenylamine-based polyimides (TPA-PI) in air and nitrogen atmosphere. The minor weight loss at about 100 °C is caused by trace H_2O.

The thermal properties of the polyimide (TPA-PI) were evaluated by DSC and TGA. TPA-PI exhibits high glass transition temperatures (Tg) at 305 ^oC and excellent thermal stability. It shows no significant weight loss below 538^oC in air and nitrogen atmosphere.

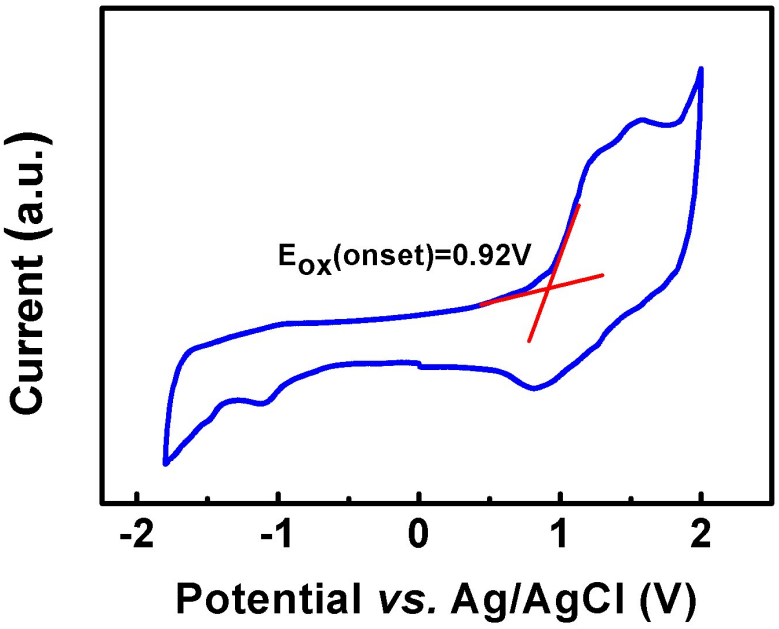

Figure S4. Cyclic voltammogram of TPA-PI.

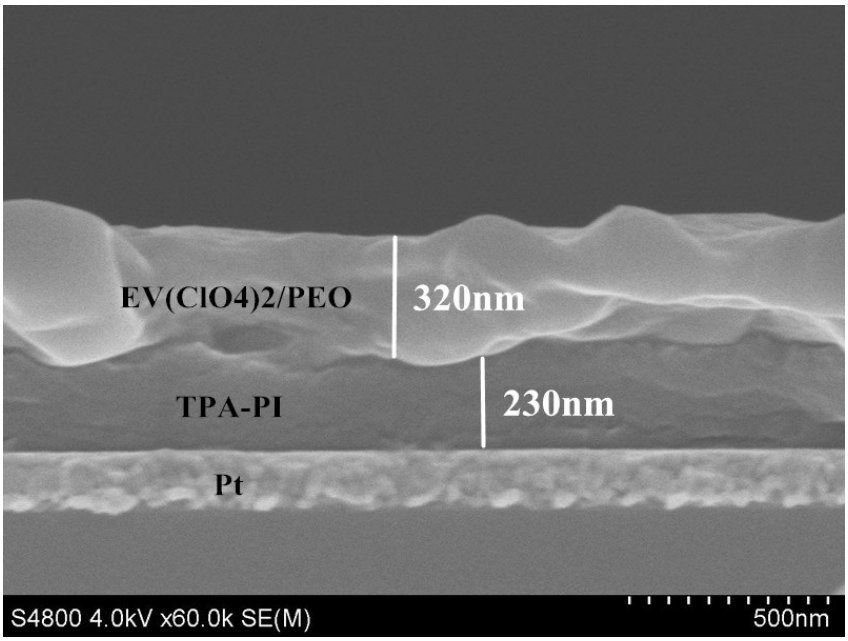

Figure S5. Cross-sectional scanning electron microscopic (SEM) image of the Ta/320 nm $EV(ClO_4)_2$/230 nm TPA-PI/Pt device.

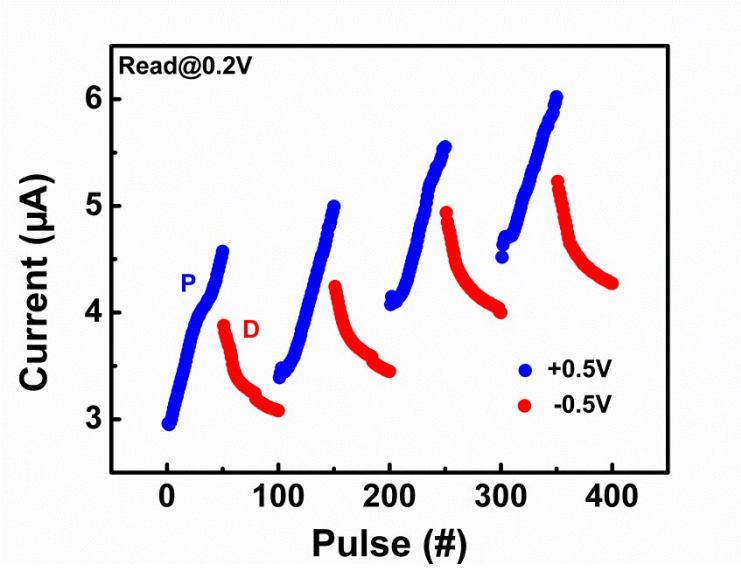

Figure S6. The reliability and reversibility of synaptic potentiation/depression characteristic.

The continuous increase and decrease of the device conductance are analogous to synaptic potentiation and depression characteristics, as shown in Fig. S6. The potentiation characteristic is caused via applying 50 consecutive positive voltage pulses (amplitude of 0.5 V, duration of 10 ms), which is ascribed to the electrochemical oxidation of TPA-PI. The depression characteristic is caused via applying 50 consecutive negative voltage pulses (amplitude of -0.5 V, duration of 10 ms), which is ascribed to the electrochemical reduction of TPA-PI radical cation. Further insight into the potentiation/depression characteristic, four potentiation/depression cycles have been achieved by consecutive positive/negative voltage pulses in Fig. S6, which shows the reliability and reversibility of synaptic potentiation/depression characteristic. From the perspective of redox processes, four potentiation/depression cycles indicate the reliability and reversibility of the redox

processes. The overall current strengthening may be due to the incomplete reduction of TPA-PI radical cation.

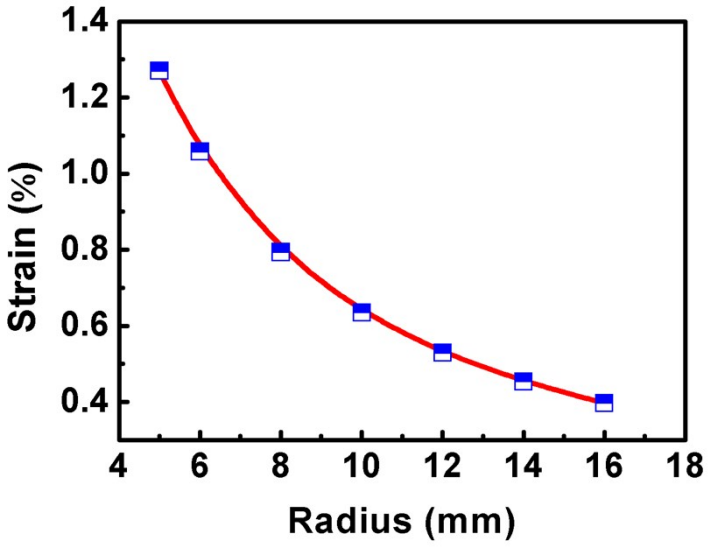

Figure S7. The strain as a function of radius.

The bended device is regarded as an ideal part of a circle at any bending radius, so the strain S induced on the surface of the bended Polymer/PET device can be estimated from following the equations:

$$S = \frac{(t_M + t_s)(1 + 2\eta + \chi\eta^2)}{2R(1+\eta)(1+\chi\eta)} \quad (1)$$

$$\chi = Y_M / Y_S \quad (2)$$

$$\eta = t_M / t_S \quad (3)$$

where t_M and Y_M are the thickness and Young's modulus of the polymer layer, t_s and Y_S are the thickness and Young's modulus of the PET substrate, and R is the curvature radius of the sample upon being bended. Since the thickness of the polymer layer is much smaller ($t_M \approx 550$ nm) than that of the PET substrate ($t_S \approx 5$ mil, or 127μm), equation (1) can be simplified as:

$$S \approx t_S / 2R \quad (4).$$

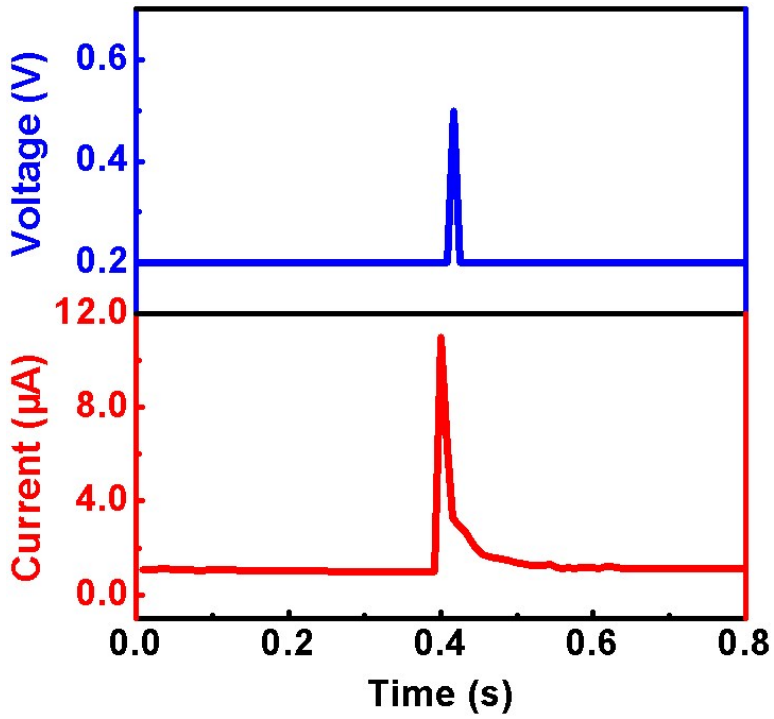

Figure S8. Excitatory postsynaptic current (EPSC) triggered by a pre-synaptic spike (0.5V, 10ms) at bending radius r= 16mm.

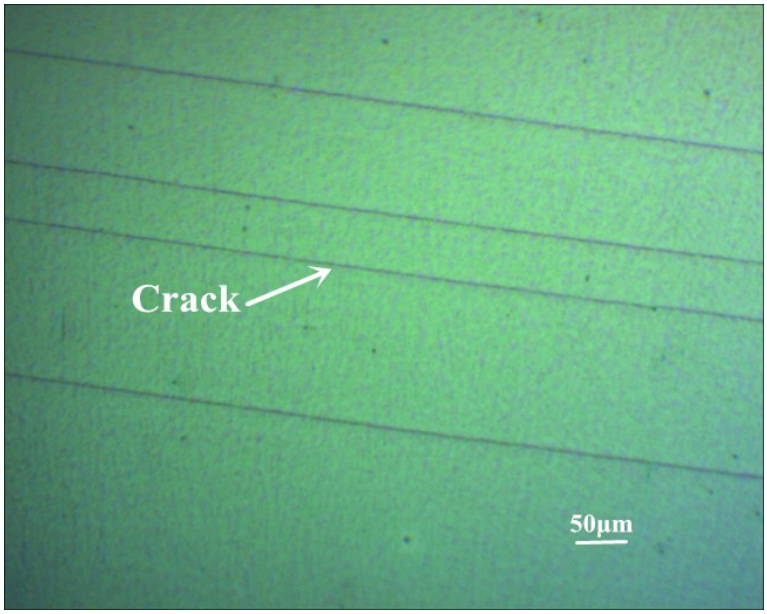

Figure S9. Optical microscope image of the Ta/EV$(ClO_4)_2$/TPA-PI/Pt/PET device with bending radius of less than 12 mm.

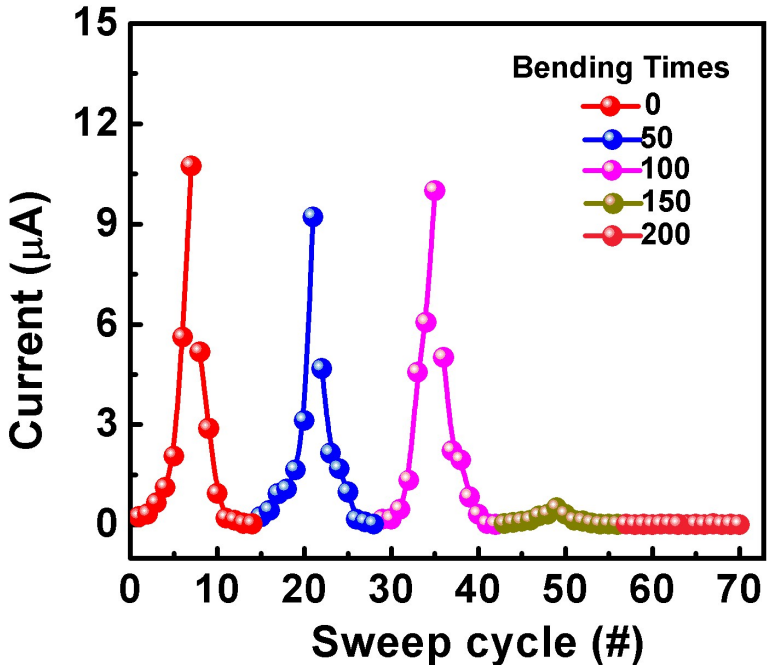

Figure S10. Variation of the electrical characteristics at different bending times (0, 50, 100, 150, 200 times). The device is bent to r = 16mm repeatedly.